Vertical Structure of Chlorophyll-a During Marine Heatwaves in the California Current Ecosystem

Jian Li[1,2,3], Arthur J. Miller[2], Dillon J. Amaya[4], Qi Wang[5], Peiliang Li[1,3,6], Yanzhen Gu[1,3,6*], Peng Bai[7]

[1]Ocean College, Zhejiang University, Zhoushan, China

[2]Scripps Institution of Oceanography, University of California, San Diego, La Jolla, USA

[3]Hainan Institute, Zhejiang University, Sanya, China

[4]NOAA/Physical Sciences Laboratory, Boulder, USA

[5]Marine Academy of Zhejiang Province, Hangzhou, China

[6]Hainan Observation and Research Station of Ecological Environment and Fishery Resource in Yazhou Bay, Sanya, China

[7]Marine Science and Technology College, Zhejiang Ocean University, Zhoushan, China

Corresponding author*: Yanzhen Gu (guyanzhen@zju.edu.cn)

Abstract

In the past decades, the California Current Ecosystem (CCE) has experienced intense marine heatwaves (MHWs), which have induced significant disruptions to local phytoplankton communities. Using 30-year CalCOFI observations, we identify a previously undocumented vertical structure in chlorophyll-a concentration (CHL) response to MHWs, characterized by CHL reductions in the surface layer coupled with increases in the subsurface. By integrating observations and coupled physical-biogeochemical model products, we demonstrate that surface CHL declines are primarily attributed to suppressed nutrient upwelled to the upper ocean. Although surface irradiance increased modestly (+3.5%), light availability in the subsurface layer improved substantially (+21.7%) due to reduced phytoplankton shading at the surface. Concurrent with enhanced lateral nutrient transport, phytoplankton growth at depth was promoted during MHWs. This study highlights the pivotal role of subsurface phytoplankton dynamics in shaping the vertical CHL structure and its variability under extreme events.

Introduction

Marine heatwaves (MHWs), defined as prolonged episodes of anomalously warm seawater temperature (Hobday et al., 2016; Oliver et al., 2021), have shown increasing frequency and intensity over the past century and are projected to intensify further under global climate change (Frölicher et al., 2018; Oliver et al., 2018). Accumulating evidence demonstrates that these extreme events exert cascading impacts on marine ecosystems, including mass coral bleaching (Eakin et al., 2019), critical habitat degradation (Smith et al., 2023), ecosystem regime shifts (Wernberg et al., 2013) and unprecedented biodiversity loss (Smale et al., 2019). Moreover, MHWs are increasingly being examined along with concurrently occurring biogeochemical extremes (Capotondi et al., 2024), such as acidity and hypoxia (Gruber et al., 2021; Hauri et al., 2024; Le Grix et al., 2025), which can exacerbate the responses of sensitive marine organisms (Hauri et al., 2024; Wong et al., 2024). Such ecological disruptions fundamentally compromise the provision of essential ecosystem services (Smith et al., 2021). Given their escalating frequency, unpredictable spatiotemporal patterns, and potentially irreversible ecological consequences, MHWs have emerged as a pressing global concern (Frölicher & Laufkötter, 2018; Holbrook et al., 2019; Smith et al., 2021).

As the foundation of marine primary production, phytoplankton regulate key biogeochemical processes including carbon sequestration, nutrient cycling, and food web dynamics (Falkowski et al., 2008; Marañón, 2015). Their biomass and community structures can be significantly influenced by MHWs due to their various sensitivities to thermal anomalies, with cascading effects on productivity and functional diversity (Barton et al., 2016; Thomas et al., 2012). Previous studies demonstrated that MHWs exert spatially heterogeneous impacts on phytoplankton across regions and events (Fernández-González et al., 2022; Le Grix et al., 2020). Generally, surface CHL decreases in the tropics and mid-latitudes while it increases at high latitudes during MHWs (Noh et al., 2022), with these patterns governed by alterations in nutrient dynamics (Fernández-González et al., 2022; Hayashida et al., 2020; Zhan et al., 2023),

light availability (Le Grix et al., 2020), and iron limitation (Peña et al., 2019). Concurrently, phytoplankton community structures tend to exhibit a universal shift toward smaller species during MHWs, altering energy transfer efficiency through marine food webs (Delgadillo-Hinojosa et al., 2020; Wyatt et al., 2022; Zhan et al., 2024; Zhan et al., 2023).

The California Current Ecosystem (CCE), where CalCOFI (The California Cooperative Oceanic Fisheries Investigations; Fig.1) is located, experienced multiple severe MHWs in recent decades, driven by synergistic atmospheric-oceanic forcing mechanisms including intensified North Pacific High variations (Amaya et al., 2020; Di Lorenzo & Mantua, 2016), reduced coastal upwelling (Wei et al., 2021), and anomalous poleward current transport (Zaba et al., 2020). Therefore, a growing body of research has documented MHW-induced impacts on phytoplankton within CCE. For example, during the 2014–2015 MHW, often called "the Blob", suppressed upwelling and intensified stratification reduced the nutrient supply to the euphotic zone, causing significant declines in phytoplankton biomass and net primary production in CCE (Cavole et al., 2016). Meanwhile, to adapt to the abnormal temperature and nutrient conditions, phytoplankton community shifted toward smaller cells (Closset et al., 2021; Delgadillo-Hinojosa et al., 2020; Landry, Freibott, Stukel, et al., 2024), and harmful algal bloom events in nearshore were also related to MHWs (Fischer et al., 2024; McCabe et al., 2016).

Increasing evidence indicates that MHWs are not confined to the surface layer but may extend to deeper waters (Capotondi et al., 2024; Zhang et al., 2023), with potentially increased duration and intensity in some case (Köhn et al., 2024; Plume et al., 2025). Therefore, vertically propagating extremes represent an emerging topic in recent MHW research (Le Grix et al., 2025; Wong et al., 2024). These studies revealed that the subsurface compound events (MHW, low oxygen and high acidity) are often associated with vertical displacements of water masses, have shown significantly intensification in the decades (Wong et al., 2024), and are projected to be enhanced under global

warming (Le Grix et al., 2025). However, the vertical response of phytoplankton communities to MHWs remains relatively understudied due to limited data availability (Viljoen et al., 2024; Yuan et al., 2024). Recent findings by Viljoen et al. (2024) have highlighted a pronounced decoupling between surface and subsurface phytoplankton biomass during the past decade of ocean warming in the Sargasso Sea. That study underscores the limitations of remote sensing observations and emphasizes the critical role of vertical structures in examining biogeochemical responses to extreme events.

Such vertical decoupling raises critical questions about the underlying mechanisms and whether they differ during short-term extreme events like MHWs compared to gradual, long-term ocean warming. In predominantly nutrient-limited systems like the CCE, the vertical structure of CHL exerts a more critical influence on marine biogeochemical cycling and carbon export potential than surface CHL alone (Cullen, 2015). However, our current understanding of MHW impacts on CHL remains disproportionately focused on epipelagic phytoplankton responses, leaving critical knowledge gaps regarding vertical heterogeneity in phytoplankton dynamics during extreme warming events, thereby hindering our ability to predict ecosystem resilience and climate feedback mechanisms.
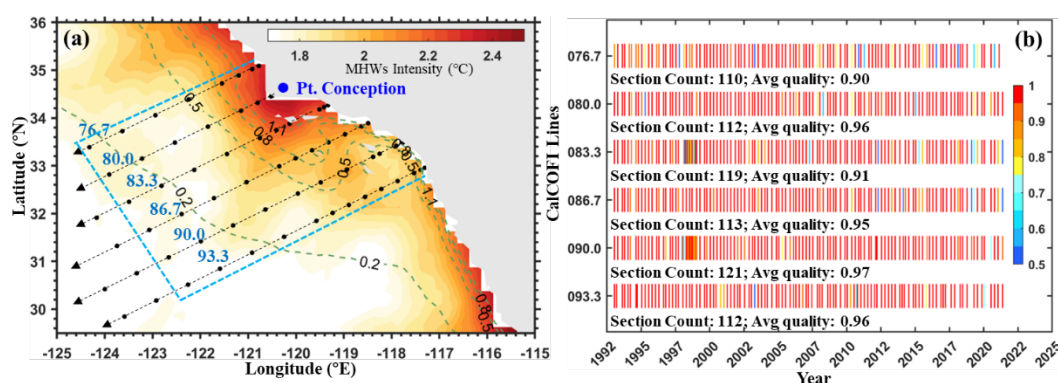

Fig.1 (a) Mean MHW intensity based on OISST from 1993 to 2022. Black dots and dashes represent the sampling stations and transect lines of CalCOFI cruises. Green dashes represent the mean surface CHL concentration from Copernicus-GlobColour (1997–2022). Blue box denotes the boundary of the CalCOFI region. (b) Sampling records and its data quality (proportion of valid data) of six CalCOFI Lines from 1993 to 2022.

In this study, we observed a previously undocumented phenomenon in the CalCOFI

region that the vertical response of CHL to MHWs is not uniform, but exhibits a distinct vertical structure characterized by negative surface anomalies overlying positive subsurface anomalies (Herein, we define the "surface" as extending from the sea surface to the subsurface chlorophyll maximum layer (SCML) depth, and the "subsurface" as the water column beneath the SCML depth). Using in situ observations from CalCOFI, we systematically characterize the vertical CHL anomaly structure and associated environmental conditions during MHWs. We further employ physical (PHY) and biogeochemical (BGC) model outputs from the Copernicus Marine Environment Monitoring Service (CMEMS) to investigate the underlying mechanisms driving this vertical pattern. This study aims to advance our understanding of vertically response of phytoplankton to MHWs and provide novel insights into their ecological consequences in upwelling systems.

Results

MHWs in CCE region

In the past 30 years (1993–2022), intense MHWs were predominantly concentrated along the coastal CCE region that contains the highest phytoplankton biomass (Fig.1a), particularly around Point Conception, where the averaged MHWs intensity exceeds 2.3°C. Correspondingly, this region experiences severe declines in surface CHL (Fig.S6 in the Supplementary Information). To characterize the temporal evolution of these events, we further examined the monthly mean MHWs intensity and spatial coverage of the study area (blue box in Fig.1a), as a function of time. The results (Fig.2a) indicate that the most severe and frequent events occurred during positive Pacific Decadal Oscillation (PDO) years (Fig.2b), which are typically associated with suppressed coastal upwelling and increased net downward surface heat flux (Ren et al., 2023). Here, a given month is labeled as "MHW month" if more than 50% of the study area experiences MHW condition and the regional mean intensity exceeds 1 °C. Based on this definition, a total of 68 MHW months were identified between 1993 and 2022. Among these, 23 CalCOFI cruises (∗ in Fig.2) were conducted under MHWs in CCE,

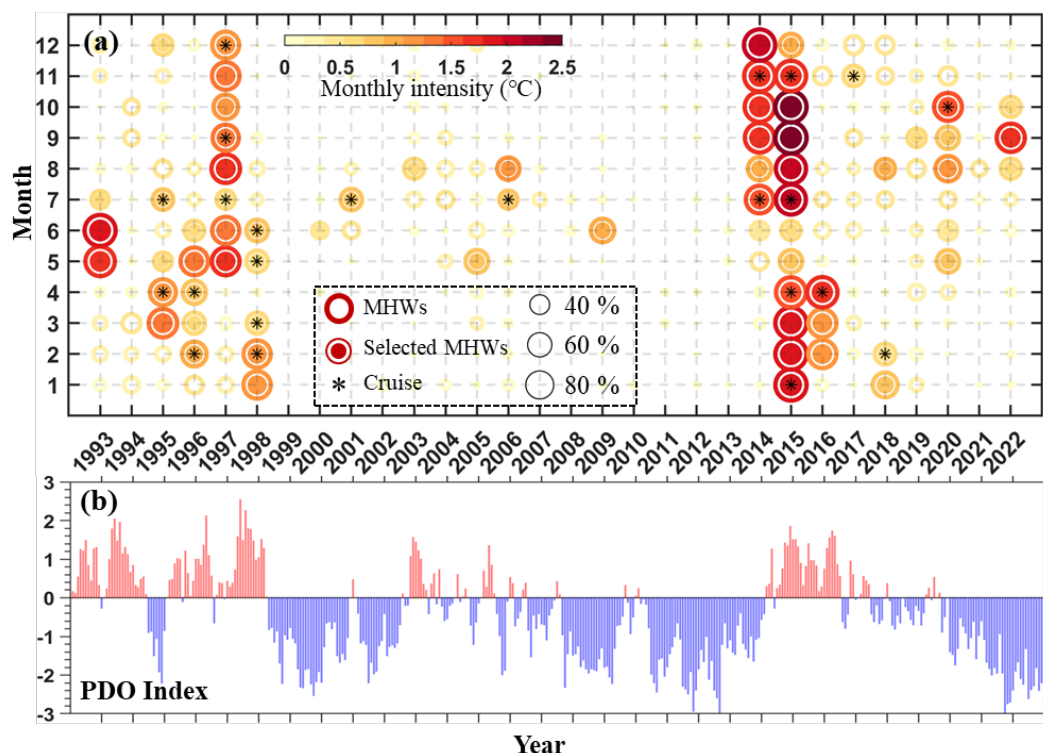143 providing valuable in situ observations to assess ecosystem responses to extreme

144 warming.

145

146 **Fig.2 (a) MHW occurrences in the CalCOFI region based on OISST. Color and radius of**
147 **unfilled circles represent the monthly mean intensity and spatial coverage (%) of MHWs,**
148 **respectively. Filled circles indicate months when more than 50% area (Fig.1) is under MHW**
149 **conditions and the regional mean intensity exceeds 1 ℃, labeled as "MHW month". Asterisks**
150 **denote MHW months when CalCOFI cruises were conducted. (b) Pacific Decadal Oscillation**
151 **(PDO) Index.**

Vertical CHL responds to MHWs

153 Based on 687 sections derived from 6 CalCOFI cruise lines collected between 1993 and

154 2022, we computed CHL anomalies (N = 35754) within the 200-m depth water column

155 during MHWs (filled circles with asterisks in Fig.2) to examine the vertical response

156 of CHL to these extreme events (Fig.3a). Intriguingly, we observed an unexpected

157 vertical structure in the CHL pattern, characterized by negative anomalies in the surface

158 layer accompanied by positive anomalies at depth, which has rarely been captured in

159 this region by previous studies relying on satellite observations or vertically integrated

160 investigations. In order to better quantify this phenomenon, we further assessed the

vertical distribution of CHL anomalies at each depth level within the CalCOFI region (Fig.3b). The results reveal a significantly reduction in CHL (mean: 0.08–0.15 μg/L) from surface to 50 m depth, with a concurrent increase (0.01-0.05 μg/L) below 70 m depth during MHWs. The maximum negative anomalies occur at depths of 20–40 m, while the most pronounced positive anomalies were located around 70–80 m depth. Although the magnitude of subsurface positive anomalies was much smaller at individual depths compared to surface negative anomalies, their cumulative effect remains substantial when vertically integrated (-2.85 μg/L at surface versus 1.62 μg/L at subsurface, exceeding 50% of the surface reduction magnitude), presenting a non-negligible contribution when estimating variability of vertically integrated CHL. This vertical redistribution may help explain why no significant correlations were previously found between MHW intensity/duration and vertically integrated CHL (Chen et al., 2024), despite surface CHL showed strong statistically significant correlations with MHWs. It may also elucidate the unexpected positive depth-integrated CHL anomaly during 2015-2016 El Niño in the CCS (McClatchie et al., 2016).
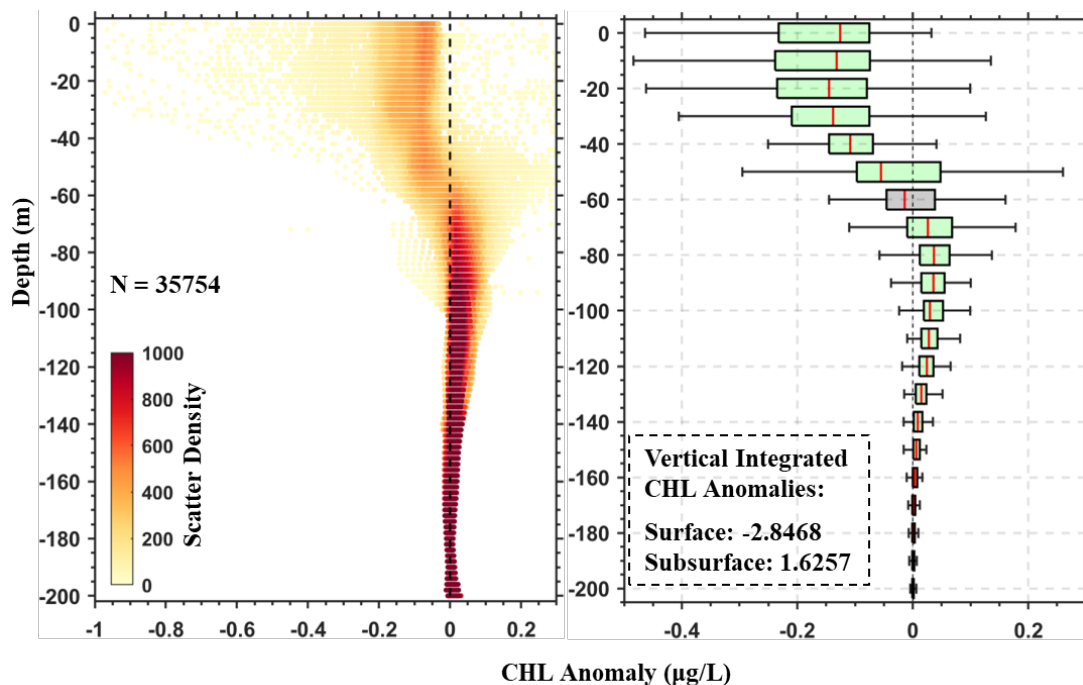

Fig.3 (a) Scatter density plot of CHL anomalies during MHWs, derived from vertical profiles at all stations across six CalCOFI lines. (b) Boxplot of CHL anomalies at 10-m depth intervals. The vertical dashed line indicates zero anomaly, and red lines denote the median. Green boxes

indicate depths where anomalies are statistically different from zero (T-test; $p < 0.05$). Vertically integrated CHL anomalies were calculated separately for the surface layer (from surface to SCML depth) and the subsurface layer (SCML depth to 200-m) at each station, and then averaged across all stations within the CalCOFI region.

Since this phenomenon was consistently observed across all CalCOFI transects, we selected Line 90.0 for detailed analysis due to its relatively higher sampling density and superior data quality (Fig.1b; described in the Data and Methods) to better understand the vertical structure of the CHL anomalies. Composite anomalies of all variables shown in Fig.4 and Fig.5 were averaged over MHW months during which CalCOFI cruises were conducted (asterisks in Fig.2).

Composite temperature anomalies across four seasons show that the most intense warming events happened during winter and fall (Plume et al., 2025). Previous studies have demonstrated that vertical advection, which is associated with wind-driven reduced upwelling (Capotondi et al., 2024; Cervantes et al., 2024; Dalsin et al., 2023; Fewings & Brown, 2019; Plume et al., 2025; Zhan et al., 2024; Zhang et al., 2023) and deepened thermocline (Wei et al., 2021), constitutes the dominant driver of MHW development in the CCE. Thus, warming signals are observed in the subsurface across all four seasons, with particularly intensified warming at depth during winter due to weak stratification (Köhn et al., 2024; Plume et al., 2025). Fig.4e-h illustrate the seasonal distributions of CHL anomalies along Line 90.0, offering insight into phytoplankton responses to MHWs. This vertically decoupled variability was detected across all seasons, extending from onshore to offshore regions. The maximum reduction in CHL occurs around the SCML depth (red dashed lines in Fig.4e-h), whereas CHL exhibited anomalous increases below the SCML during warming events. Due to the varying nutrient and physical environments between onshore and offshore, the SCML does not occur at a fixed depth but deepens as the offshore distance increases. Consequently, layers around 60-m depth (gray bar in Fig.3b) contain positive anomalies onshore but negative anomalies offshore, resulting in no statistically significant change during MHWs when anomalies are depth-aggregated.
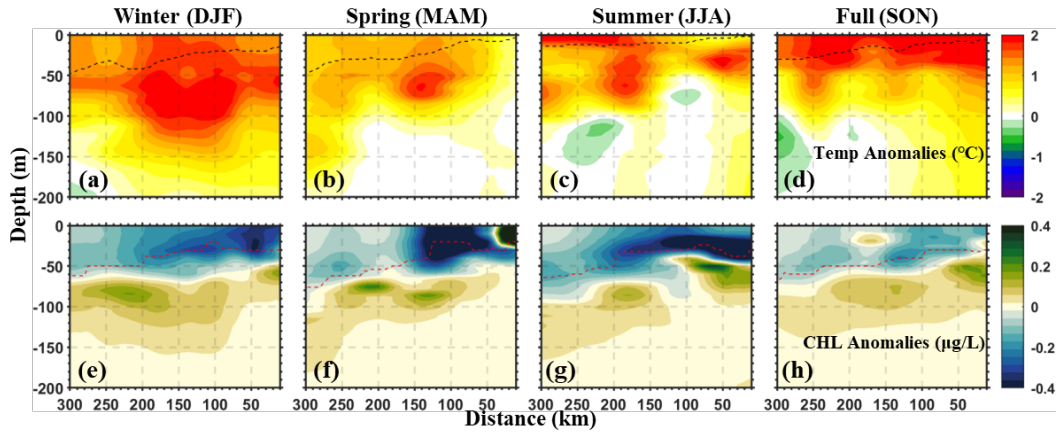
Fig.4 Seasonal anomalies of temperature (a-d) and CHL (e-h) during MHWs along CalCOFI Line 90.0 (DJF, MAM, JJA, SON represent winter: December–February, spring: March–May, summer: June–August, and fall: September–November, respectively). Black and red dashed lines denote mixed layer and subsurface chlorophyll maximum layer (SCML) depth, respectively. Anomalies were calculated based on data from MHW months during which CalCOFI cruises were conducted (asterisks in Fig.2)

This finding highlights a decoupled vertical structure in CCE phytoplankton dynamics during MHWs, whereby subsurface phytoplankton biomass anomalies contradict the conventional paradigm of the reduced CHL pattern. The significant negative anomalies of surface CHL, which have been widely reported in the CCE, were mainly driven by reduced nutrient availability due to weakened upwelling (Landry, Freibott, Beatty, et al., 2024; Landry, Freibott, Stukel, et al., 2024; Zhan et al., 2024). However, the subsurface positive anomalies have rarely been documented, and the underlying mechanism remains unclear, challenging our understanding of MHW-induced ecological disturbances in the CCE. Therefore, the remainder of this study focuses on elucidating the mechanisms governing subsurface CHL enhancement during MHWs in this eastern boundary upwelling system.

Environmental Anomalies During MHWs

Vertical variability in CHL is regulated by both hydrodynamic and biogeochemical processes (Cullen, 2015). Thus, we examined the variability of key environmental variables during MHWs along CalCOFI Line 90.0 (Fig.5a-h) to explore the potential drivers of subsurface CHL anomalies. Composite temperature anomalies reveal that the

232 most intense warming occurs 100-200 km offshore, extending from the surface to the

233 ~100 m depth. In addition, salinity significantly increased in the upper 100 m layer,

234 possibly due to the enhanced evaporation from warmer seawater or to weakened

235 transport of fresher waters from the north. Below 100 m depth, salinity shows a negative

236 anomaly at a similar distance (100–200 km from the coast), and its distribution indicates

237 that the negative salinity anomaly originates from deeper layers. According to the

238 abovementioned mechanism of the MHWs in this region as well as the distribution of

239 warming signal, these salinity anomalies indicate a reduction in the upward transport

240 of salt deep water–consistent with suppressed upwelling. Additionally, negative salinity

241 anomalies near the offshore boundary of the transect imply that lateral intrusions may

242 also contribute to the observed freshening, as projections under future warming

243 scenarios have indicated (Rykaczewski & Dunne, 2010).

244
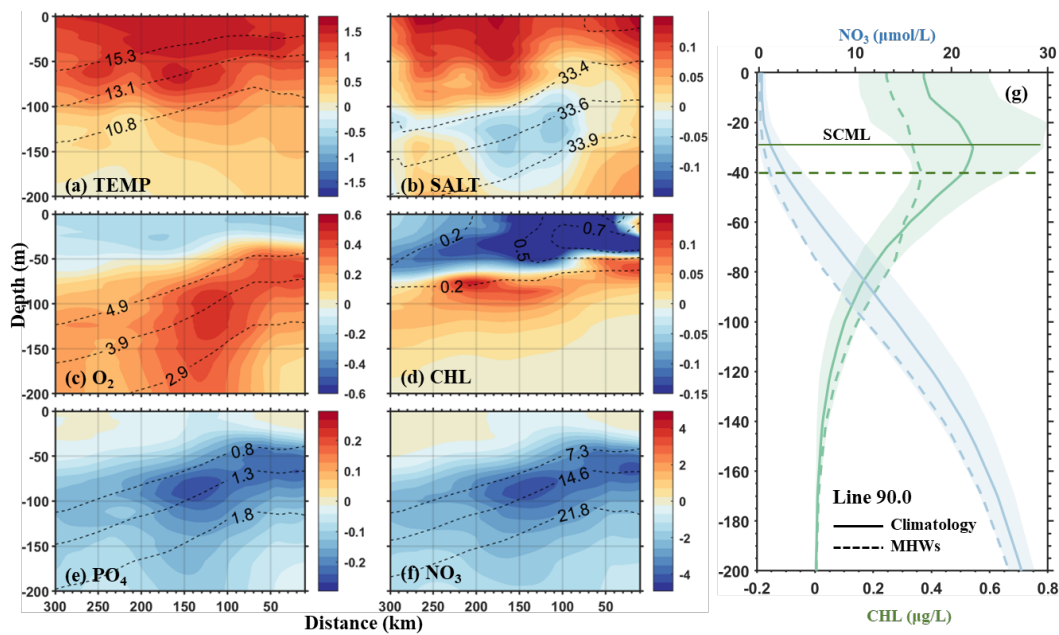
Fig.5 (a-f) Composite anomalies of temperature (TEMP; °C), salinity (SALT; PSU), dissolved oxygen (O$_2$; ml/L), CHL (µg/L), phosphate (PO$_4$; µmol/L) and nitrate (NO$_3$; µmol/L) during MHWs, with contours representing climatological values. (g) Vertical profiles of CHL (green), SCML (dark green) and nitrate concentration (blue) under climatology (solid lines) and MHWs (dash lines) states, averaged along offshore distance of CalCOFI Line 90.0.

250 For the nutrient environment, as expected, phosphate and nitrate show consistent

251 declining patterns along their respective isolines throughout the water column during

252 MHWs, with the strongest reductions occurring between 50 and 100 m depth,

253 coinciding with the depths of maximum CHL positive anomalies. Along the cross-shore

254 direction, nutrient depletion was most pronounced between 100 and 200 km from the

255 coast, where suppressed upwelling occurred. These nutrient patterns likely reflect a

256 combined effect of weakened upwelling and enhanced consumption by increased

257 subsurface phytoplankton biomass. Positive oxygen anomalies exhibited a similar

258 subsurface pattern with the nutrients, further supporting the interpretation that observed

259 nutrient reductions are driven by both physical and biogeochemical processes. Notably,

260 other biogeochemical processes, such as the remineralization and grazing, may also

261 contributed to the patterns of CHL, oxygen and nutrients during MHWs. However, in

262 this study, we mainly focus on the possibly variations driving by the growth and

263 mortality of the phytoplankton.

264 Overall, compared with climatological conditions, the SCML deepened by

265 approximately 8 m (Fig.5i), and the average nitracline depth (defined as the depth where

266 nitrate concentration first exceeds 1 μmol/L) also deepened from 21 to 33 m depth

267 during MHWs. Such shifts are consistent with prior findings in this region (Chen et al.,

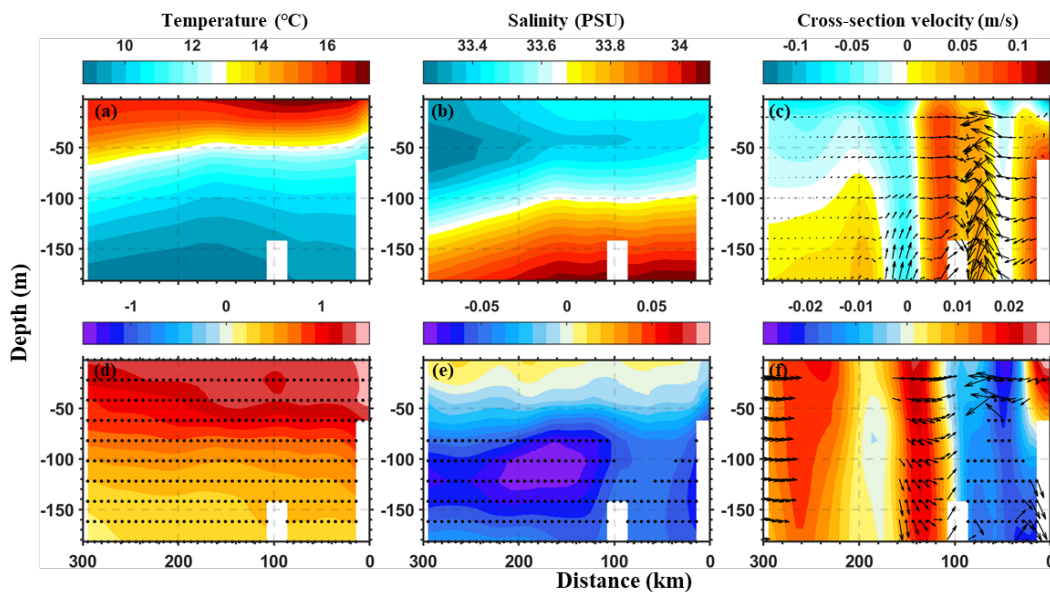268 2024; Landry, Freibott, Beatty, et al., 2024).

269

270 **Fig.6 Climatological (a-c) profiles of temperature, salinity and cross section velocity and their**

composite anomalies (d-f) during MHWs along CalCOFI Line 90.0. Black dots denote the anomalies are significantly different from zero (T-test; $p < 0.05$). Arrows in (c) and (f) represent the mean along-section and vertical velocities and their anomalies (only shown when anomalies in both directions are significantly different from zero), vertical component of velocity is multiplied by 1000 for better visualization. Note that the composite anomalies are calculated by the same MHW month as Fig.5.

To further support our descriptions of local physical and biogeochemical variability, we incorporated output from CMEMS BGC and PHY numerical models. Prior to utilizing BGC-derived variables, we conducted comprehensive validation against satellite and in-situ observations (see Text S1 in the Supplementary Information). In general, the model demonstrates satisfactory performance in simulating CHL dynamics within the study region (Fig.S1-S2) and, critically, it successfully reproduces the vertically decoupled CHL structure and associated nutrient-oxygen patterns observed during MHWs (Fig.S3), showing good agreement with the CalCOFI data (Fig.5). Outputs from the PHY model were not further validated, as its skill has been well established in this region (Alexander et al., 2023; Amaya et al., 2023; Amaya et al., 2020).

Vertical profiles of simulated physical variables clearly reproduce the key dynamic processes described above (Fig.6). Maximum salinity anomalies occurring 100–200 km offshore below 100 m depth exhibit clearer extension both towards the depth and further offshore (Fig.6e). A significant upwelling zone indeed exists within this offshore band, with its intensity significantly reduced during MHWs (Fig.6f). Additionally, enhanced eastward advection was also observed offshore, potentially transporting fresher waters toward the upwelling region. Notably, anomalies in Fig.6 were computed as the deviations from monthly climatology (whereas those in Fig.5 are based on seasonal climatology derived from observations).

Discussion

The subsurface environmental conditions described above explain the mechanisms driving the observed positive CHL anomalies. While the composite patterns in nutrients and oxygen anomalies likely result from weakened upwelling combined with enhanced

phytoplankton activity, they do not directly account for the positive anomalies in subsurface phytoplankton biomass. To better understand the drivers of enhanced subsurface CHL during MHWs, it is necessary to further investigate the event-scale dynamics shaping this response. We therefore focused on the representative 2014–2015 MHW in the CCE to investigate the key mechanisms underlying this vertical structure.

Case study of the 2014–2015 MHW in the CCE

Unlike the large-scale North Pacific warming event ("the Blob"), the 2014–2015 MHW along the California Coast are primarily driven by intermittent air-sea heat flux, horizontal and vertical heat advection anomalies (Zaba & Rudnick, 2016; Zaba et al., 2020). Specifically, MHW in 2014 was driven by both anomalous vertical heat advection and air-sea heat flux (Zaba & Rudnick, 2016), whereas in 2015, alongshore heat advection (increased poleward volume transport and warmer-than-average temperature of the California Undercurrent) also contributed to the anomalous warming, in addition to the aforementioned drivers (Zaba et al., 2020). In addition, both years featured notable positive cross-shore heat advection anomalies (Zaba et al., 2020). With the primary physical drivers of the 2014–2015 MHW established, we next investigate the vertical CHL dynamics and associated environmental parameters within the CalCOFI region (Fig.7). Anomalies are calculated as deviations from monthly climatology (averaged over the CalCOFI region), with long-term signals (more than 5 years) removed using a high-pass Butterworth filter.
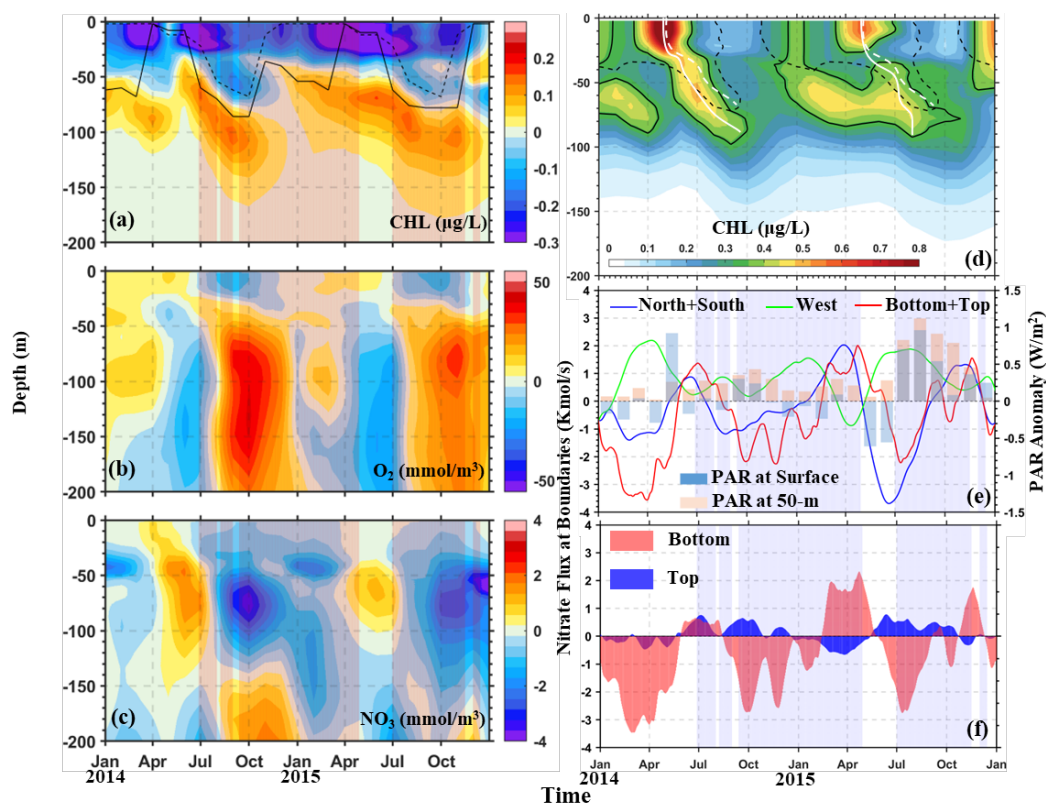
Fig.7 (a-c) Vertical anomalies of simulated CHL, dissolved oxygen and nitrate, averaged over the CalCOFI region, shown as a function of time. Dashed and solid lines in (a) refer the climatological and real SCML depth, respectively. (d) Vertical CHL distribution from 2014 to 2015. Dashed and solid contours (white lines) represent the climatological and real 0.4 µg/L CHL isoline (SCML), respectively. PAR at surface is divided by 5 for visualization. (e) Nitrate flux anomalies across the five boundaries of the CalCOFI region: alongshore (blue), cross-shore (green), and vertical (red), with positive values indicating inward transport. Blue and red bars denote anomalies of PAR at the surface and 50-m depth, respectively. (f) Nitrate flux anomalies across bottom and top boundaries.

Model simulations revealed that positive subsurface CHL anomalies initially occurred around 50 m depth and progressively deepened to ~150 m as the MHW developed (Fig.7a). More specifically, the seasonal chlorophyll bloom that typically originates in April 2014 and persists through August in climatology, was suppressed before July due to MHW disruption (solid and dashed black contours in Fig.7d). Concurrently, phytoplankton exhibited deeper and more pronounced subsurface growth (solid and dashed white lines in Fig. 7d), contributing to the positive anomaly. This anomaly attenuated with the seasonal shoaling of the SCML around November (black lines in Fig.8a). During a subsequent proliferation phase in January 2015 (Fig. S5), surface

339 productivity was again suppressed under stronger MHW conditions (Fig. S4), with

340 enhanced growth occurring below 50 m depth.

341 Our analysis of environmental variable anomalies in the CCE, integrated with

342 established theoretical frameworks of phytoplankton dynamics (Cullen, 2015; Landry,

343 Freibott, Beatty, et al., 2024; Landry, Freibott, Stukel, et al., 2024; Zhan et al., 2023;

344 Zheng et al., 2024), suggests that nutrient dynamics is a primary driver governing

345 vertical CHL variability. However, the phytoplankton biomass would be expected to

346 decline rather than show positive anomalies as the SCML deepens due to reduced

347 nutrient availability in deep waters (Beckmann & Hense, 2007). In such cases, light

348 availability may become another dominant factor, especially when phytoplankton grow

349 below the climatological euphotic depth. In highly productive coastal system like CCE,

350 underwater light conditions depend not only on surface irradiance but also on vertical

351 light penetration, which is strongly influenced by water turbidity and the phytoplankton

352 self-shading effect (Kavanaugh et al., 2009; Shigesada & Okubo, 1981). Thus, we

353 quantified the Photosynthetically Active Radiation (PAR), and nitrate flux across the

354 five boundaries of the CalCOFI region (Fig.7f) to further assess the contributions of

355 light availability and nutrient supply to the subsurface CHL during MHWs. Surface

356 PAR data were obtained from the MODIS PAR product, while subsurface PAR was

357 calculated using the same three-waveband light penetration scheme as CMEMS-BGC

358 model. Advection and diffusion are the major physical processes that control the nitrate

359 flux in the water column. In upwelling system like the CCE, the contribution of

360 diffusion is generally considered minor compared to advection (Moreira-Coello et al.,

361 2017; Mouriño-Carballido et al., 2021). Thus, we mainly focus on the advection term

362 in this study.

363 Positive nitrate anomalies were observed between 50 and 100 m depth prior to the onset

364 of both MHWs in June 2014 and 2015 (Fig.7c), potentially creating a more favorable

365 nutrient environment for phytoplankton growth here. Nitrate flux calculations revealed

366 positive anomalies across all three spatial dimensions (cross-shore: westward;

367   alongshore: northward + southward; vertical: upward + downward) in June 2014, and

368   the positive vertical flux resulted from both enhanced import through the bottom

369   boundary and reduced export through the upper boundary. In June 2015, elevated nitrate

370   input occurred primarily through vertical and cross-shore transport (Fig.7f).

371   Subsequently, nitrate anomalies for both events diminished as the MHW progressed,

372   with vertical and alongshore nitrate flux anomalies turning negative. Positive cross-

373   shore nitrate fluxes were observed during nearly all events between 2014 and 2015,

374   closely aligning with net heat advection in the same direction (Zaba et al., 2020).

375   Regarding the light conditions, significantly positive PAR anomalies were observed at

376   50 m depth throughout the 2014–2015 events, while sustained surface PAR

377   enhancement occurred during the latter event (July to December 2015). Compared to

378   the surface, subsurface PAR showed stronger correspondence with the vertical

379   distribution of positive CHL anomalies, which exhibited progressive deepening in

380   response to two distinct phases of subsurface PAR enhancement (June–October 2014

381   and January–September 2015). These results indicate that, although the subsurface light

382   condition can be directly influenced by the surface irradiance, phytoplankton

383   productivity at depth is more sensitive to light availability within these specific layers,

384   and the self-shading effect of the phytoplankton can significantly alter the light

385   penetration throughout the water column during MHWs. While the depth of the positive

386   CHL anomalies aligned well with the PAR anomalies at 50-m depth, light availability

387   alone cannot fully explain the observed subsurface phytoplankton activity. For example,

388   the positive subsurface CHL anomaly reached its maximum intensity at 60 m depth in

389   May 2015, despite the absence of significant subsurface PAR enhancement. In this case,

390   enhanced productivity was primarily supported by positive nitrate anomalies

391   transported via upwelling and cross-shore advection. Specifically, when along-shore

392   and vertical nitrate flux anomalies were negative in June and July 2015, nitrate

393   anomalies still remained positive due to cross-shore nitrate flux supply, suggesting the

394   non-negligible contribution of lateral nutrient supply during warming events.

These findings suggest that light condition variations induced by atmospheric processes and phytoplankton self-shading effect might influence both the depth and intensity of subsurface phytoplankton growth during MHWs. However, vertical and cross-shore nitrate fluxes act as critical additional drivers sustaining subsurface productivity under these anomalous conditions.

Background Condition During MHWs

Building upon the detailed examination of specific 2014–2015 MHW events in the CCE, we further investigated the background states of these potential controlling factors during all MHWs from 1993 to 2022. Mean net nitrate flux anomalies across the five boundaries during MHWs are shown in Table 1. Compared to climatological conditions, a significant net influx of nitrate was observed from the western boundary during MHWs (1.90 kmol/s; $P < 0.01$), while no significant anomalies were found at the northern or southern boundaries. Vertically, less nitrate (-1.02 kmol/s; $P < 0.01$) was upwelled into subsurface water through the bottom boundary and reduced nitrate (-0.38 kmol/s; $P < 0.01$) was exported through the top boundary, reflecting to the suppressed upwelling during MHWs. These results suggest that, although vertical nutrient supply was substantially weakened, increased lateral input from the western boundary partially offsets the overall nutrient deficit. It can be anticipated that without this supplementary input, local nutrient levels and thus phytoplankton productivity, would likely have declined even further. This finding aligns with previous projections based on climate models, which suggest that climate-driven increases in nutrient-rich water transport through the western boundary could enhance productivity in the CCE under future warming scenarios (Rykaczewski & Dunne, 2010). Our results, derived from observed extreme warming events, support this type of local mechanism and underscore the pivotal role of lateral nutrient transport in sustaining ecosystem productivity under MHW conditions.

Table 1. Net nitrate flux anomalies (unit: kmol/s) at five boundaries and their p-values (T-test), directions into the CCE region are positive.

Boundary	South	North	West	Bottom	Top
Net Nitrate Flux Anomalies	1.81	-0.83	1.90	-1.02	0.38
P-value	0.11	0.40	< 0.01	< 0.01	< 0.01

Moreover, light condition in the subsurface layers showed varying degrees of enhancement under MHWs (Fig.8a), particular during 2014–2016 MHW, the average PAR increment throughout the water column exceeded 4 W/m^2. In order to further examine whether this light enhancement result from increased surface irradiance influenced by atmospheric processes, or reduced self-shading effect of the suppressed surface phytoplankton biomass, we examined PAR at two layers for every event. As shown in Fig.8b, most MHW months exhibited positive PAR anomalies at 50 m depth, with only two exceptions showing negative values. Surface PAR also increased in the majority of events. On averaged, surface PAR in the CalCOFI region increased by 3.53% ($p < 0.01$; T-test), likely due to reduced cloud cover and enhanced incoming solar radiation (Myers et al., 2018). However, the reduction of the surface phytoplankton significantly enhanced the light penetration in the water column, causing the subsurface PAR to significantly increase by 21.7%, which provide better light availability for the phytoplankton growth at depth. Further support for this mechanism comes from the co-location of normalized CHL and PAR anomalies during MHWs. Specifically, positive CHL anomalies emerged at depths where normalized PAR anomalies reached their maximum (shaded purple area in Fig.8b), highlighting the tight coupling between subsurface light availability and phytoplankton growth.
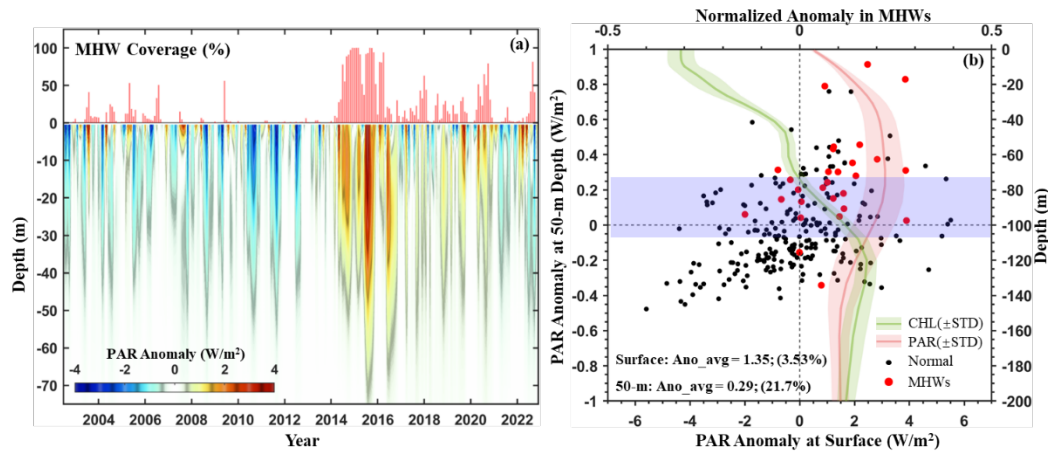
Fig.8 (a) Timeseries of vertical light conditions. Red bars represent the monthly coverage of the MHW area (%). Shading denotes the PAR anomalies at different depth. (b) Black (red) dots represent the monthly PAR at surface and at 50-m depth under normal (MHW) condition. Green and red line refer normalized anomalies of CHL and PAR under MHWs. All values here are regionally averaged over the CalCOFI region.

Thus, the mechanisms underlying the vertical structure of CHL response to MHWs in the CCE become evident. Suppressed upwelling limits the nutrient delivery to surface waters, leading to a marked decline in surface CHL. Simultaneously, enhanced lateral advection of nutrient-rich waters through the western boundary provides an additional nutrient source to the subsurface layers. Improved light penetration driven by decreased surface phytoplankton biomass, combined with increased surface irradiance, further enhance light availability in subsurface waters. The co-occurrence of lateral nutrient supply and improved light conditions promotes phytoplankton growth at depth, ultimately driving the anomalous enhancement of subsurface CHL during MHWs in the CCE.

However, despite the supplementary lateral input, composite nutrient anomalies during MHWs remain negative, suggesting that lateral nutrient import may not fully compensate for the reduced vertical supply. Additionally, under low-light conditions, the efficiency of nutrient utilization decreases (Cloern, 1999), meaning that intensified phytoplankton productivity at depth consumes greater amounts of available nutrients, further exacerbating local nutrient depletion.

The vertical heterogeneity in CHL responses to climate change and extreme events has attracted increasing attention very recently. For example, in the open Arctic Ocean, diatom blooms have been observed near the seafloor rather than at the surface, owing to improved light conditions at depth (Shiozaki et al., 2022). In the Sargasso Sea, subsurface phytoplankton biomass became increasingly decoupled from the surface community under long-term warming and enhanced stratification, leading to pronounced subsurface CHL enrichment despite surface depletion, with total phytoplankton carbon showing an overall increase over the past decade (Viljoen et al., 2024). Similarly, phytoplankton biomass in the central tropical Indian Ocean exhibits contrasting seasonal variability between surface and subsurface layers (Hu et al., 2022). Considering the projected increase in both intensity and frequency of MHWs on global scales and in CCE region (Frölicher et al., 2018; Gomes et al., 2024; Oliver et al., 2018), developing a comprehensive understanding of vertical CHL dynamic during MHWs is crucial for predicting ecosystem responses under future ocean climate scenarios.

Conclusion

In this study, we integrated long-term CalCOFI cruise observations, satellite remote sensing data, and coupled physical-biogeochemical model products to investigate the vertical CHL response to MHWs in the CCE. Our results revealed that the vertical response of CHL to MWHs is not uniformly decreased, but exhibits vertical structure with decreases in the surface layer and increases in the subsurface layer. This pattern is inherently challenging to detect through satellite-based observations. Consistent with previous studies, the reduction in surface CHL is primarily attributed to suppressed nutrient supply due to weakened upwelling. In contrast, the increase of subsurface CHL is linked to two key processes: (i) enhanced lateral nutrient transport through the western boundary, which provide additional nutrient supply under low-level nutrient conditions caused by reduced upwelling; (ii) improved light availability at depth, resulting from both increased surface irradiance and enhanced light penetration due to reduced surface phytoplankton biomass.

491   To date, satellite remote sensing remains the most effective way to monitor
492   phytoplankton dynamics in various spatial scales. However, it is inherently limited to
493   near-surface signals and may miss significant subsurface variability, where
494   phytoplankton communities are often more abundant and more sensitive to
495   environmental perturbations (Viljoen et al., 2024). Our findings suggest that subsurface
496   phytoplankton may play an important role in shaping the vertical CHL structure and its
497   response to extreme climate events. These insights provide valuable perspectives for
498   interpreting biogeochemical variability and assessing ecosystem responses across
499   trophic levels under future ocean warming scenarios (Chen et al., 2024; Iglesias et al.,
500   2024).

501   Finally, we must acknowledge the limitations of this study, particularly our exclusion
502   of biological processes such as zooplankton grazing and physiological behavior of
503   phytoplankton, which remain difficult to observe and simulate accurately. Further,
504   enhanced in-situ observations, such as those carried out by the CCE-LTER in process
505   cruises (Ohman et al., 2013); Stukel et al., 2025), and systematic sensitivity experiments
506   using advanced coupled physical-ecological models in the CCE (Cordero-Quirós et al.,
507   2022; Cordero-Quirós et al., 2019; Franks et al., 2013; Miller et al., 2015) are necessary
508   for comprehensive quantification of the regulatory mechanisms governing these
509   complex vertical CHL dynamics during MHWs.

Data and Methods

In Situ Sampling Data

512   In situ observations were obtained from the bottle database collected during quarterly
513   CalCOFI cruises, including 6 transect lines (93.3 to 76.7) in the CCE (Fig.1a). Vertical
514   profiles of seawater temperature, salinity, dissolved oxygen, chlorophyll-a
515   concentration and nutrients (phosphate, nitrite) from 1993 to 2022 were analyzed. The
516   anomalies of these environmental variables during MHWs were computed as deviations
517   from seasonal climatology for each transect.

518   Although CalCOFI generally conducts four cruises per year, sampling frequency has

519   varied due to occasional cancellations or additions (e.g., monthly sampling along Line

520   90.0 in 1998). Among all lines, Line 90.0 recorded the highest number of valid transects

521   (121; Fig. 1b).

522   To further evaluate the quality of observed CHL data, we first interpolated vertical

523   chlorophyll-a profiles from each station onto a standardized 0–200 depth grid. Depths

524   with valid data were marked as 1, and those without data were marked as 0. For each

525   station, depths that contained valid data in at least three cruises were defined as

526   climatologically valid layers. The quality of each profile was then calculated as the

527   percentage of these valid layers that were successfully sampled during a given cruise.

528   Results showed that Lines 80.0, 86.7, 90.0, and 93.3 had consistently high data quality,

529   with Line 90.0 standing out due to both dense sampling and superior quality. Therefore,

530   we selected Line 90.0 for detailed analysis.

Satellite Surface CHL Data

531   **Satellite Surface CHL Data**

532   Surface CHL data were derived from the Copernicus-GlobColour multi-sensor merged

533   product (OCEANCOLOUR_GLO_BGC_L4_MY_009_104), integrating observations

534   from SeaWiFS, MODIS, MERIS, OLCI, and VIIRS sensors. It provides daily 4-km

535   resolution surface CHL from Aug 1997 to present, and has been widely employed both

536   for global and regional CCE applications (Mélin et al., 2016; Stone et al., 2020).

Physical and Biogeochemical Model Outputs

537   **Physical and Biogeochemical Model Outputs**

538   To further investigate the dynamic mechanisms underlying this MHWs phenomenon,

539   higher-resolution fields were required. Therefore, we incorporated model outputs from

540   the Copernicus Marine Environment Monitoring Service (CMEMS) to assist our

541   analysis. The physical reanalysis product (hereafter referred to as CMEMS-PHY)

542   utilized   here   was   derived   from   eddy-resolving   GLORYS12V1   system

543   (GLOBAL_MULTIYEAR_PHY_001_030), which provides data-assimilated global

544   ocean fields at a horizontal resolution of 1/12° and 50 vertical levels, spanning from

545   1993 to two months prior to the present. This product has demonstrated improved

546   fidelity in simulating physical processes in the CCE region (Amaya et al., 2023), and

547   can therefore provide seawater temperature, salinity and ocean currents for this study.

548   The biogeochemical model outputs (CMEMS-BGC) are obtained from the Global

549   Ocean Biogeochemistry Hindcast product (GLOBAL_MULTIYEAR_BGC_001_029),

550   which is based on PISCES model (Aumont et al., 2015) and forced by FREE-

551   GLORYS2V4 ocean physical hindcast produced at Mercator-Ocean. Notably, no

552   assimilation was applied to this BGC product. It provides daily chlorophyll-a, nitrate,

553   phosphate, silicate, dissolved oxygen and primary production on a uniform 0.25°

554   horizontal grid with 75 standard levels, over the same temporal extent as physical

555   product. Prior to the analysis, variables from the physical products were interpolated

556   onto the same spatial grid of the biogeochemical products to ensure consistency in data

557   format.

SST Data and MHW Identification

559   We adopted a widely used approach (Hobday et al., 2016) to define MHW periods,

560   which is when the Sea Surface Temperature (SST) exceed the 90th percentile of the local

561   climatology for at least 5 days, over the period 1993–2022. The SST data were obtained

562   from The daily Optimum Interpolation Sea Surface Temperature (OISST) analysis

563   product (Reynolds et al., 2007), with a spatial resolution of 0.25° and spanning from

564   1920 to the present. Given that the rate of acclimatization or adaptation to warmer

565   conditions is generally assumed to be lower than the current rate of ocean warming for

566   most ecosystems (Cullen, 2015; Oliver et al., 2021), we used the period from 1982 to

567   2022 as a fixed baseline for constructing the climatology. In the following discussion,

568   a month is labeled as an "MHW month" if more than 50% of the study area (Fig.1) is

569   under MHW condition and the regional mean intensity exceeds 1 °C. Note that the long-

570   term trend of SST from 1982-2022 has been removed before identification based on the

571   recommendation of (Smith et al., 2025).

Nutrient Supply and Light Availability

As nitrate is the main nutrient limiting primary production in the CCE (Rykaczewski & Dunne, 2010), we evaluated impacts of nutrient supply on CHL dynamics by quantifying net nitrate flux transported into the CalCOFI region through five boundaries, including three horizontal boundaries (south, north, west; blue box in Fig.1a) and two vertical boundaries (bottom: 200 m depth; top: 50 m depth). Nitrate fluxes were was estimated as the product of daily nitrate concentration (CMEMS-BGC) and velocity (CMEMS-PHY), integrated over the entire cross-sectional area. Notably, advective fluxes directed into the control volume are positive (i.e., poleward flow at southern boundary, equatorward flow at northern boundary, eastward flow at western boundary, upwelling at bottom boundary and downwelling at top boundary).

Light availability in this study is quantified using Photosynthetically Active Radiation (PAR). Monthly mean surface PAR from 2002 to 2022 was obtained from 4-km MODIS (Terra + Aqua; MCD18A2) PAR product, which applies a multi-temporal surface reflectance algorithm and a look-up table (LUT) approach to estimate incident PAR (Liang & Wang, 2017). Vertical PAR profiles were computed by the surface MODIS PAR, using the same three-waveband light penetration scheme (Lengaigne et al., 2007) as the CMEMS-BGC model (Aumont et al., 2015), incorporating the effects of phytoplankton biomass and self-shading based on CHL profiles from the CMEMS-BGC output.

Date Availability

CalCOFI in-situ observations used in the study were obtained from https://calcofi.org/data/oceanographic-data/bottle-database/. SST data were downloaded from National Centers for Environmental Information (https://www.ncei.noaa.gov/products/optimum-interpolation-sst). BGC and PHY model products were derived from Copernicus Marine Data Store (https://data.marine.copernicus.eu/products). MODIS surface PAR product was downloaded from https://oceandata.sci.gsfc.nasa.gov/. Light penetration module can be found at https://forge.nemo-ocean.eu/nemo/nemo/-/tree/main/src/OCE/TRA.

Reference

Alexander, M. A., Scott, J. D., Jacox, M. G., Deser, C., Amaya, D. J., Capotondi, A., & Phillips, A. S. (2023). A survey of coastal conditions around the continental US using a high-resolution ocean reanalysis. *Progress in oceanography, 216*, 103055.

Amaya, D. J., Alexander, M. A., Scott, J. D., & Jacox, M. G. (2023). An evaluation of high-resolution ocean reanalyses in the California current system. *Progress in oceanography, 210*, 102951.

Amaya, D. J., Miller, A. J., Xie, S.-P., & Kosaka, Y. (2020). Physical drivers of the summer 2019 North Pacific marine heatwave. *Nature communications, 11*(1), 1903.

Aumont, O., Éthé, C., Tagliabue, A., Bopp, L., & Gehlen, M. (2015). PISCES-v2: an ocean biogeochemical model for carbon and ecosystem studies. *Geoscientific Model Development Discussions, 8*(2), 1375-1509.

Barton, A. D., Irwin, A. J., Finkel, Z. V., & Stock, C. A. (2016). Anthropogenic climate change drives shift and shuffle in North Atlantic phytoplankton communities. *Proceedings of the National Academy of Sciences, 113*(11), 2964-2969.

Beckmann, A., & Hense, I. (2007). Beneath the surface: Characteristics of oceanic ecosystems under weak mixing conditions–A theoretical investigation. *Progress in oceanography, 75*(4), 771-796.

Capotondi, A., Rodrigues, R. R., Sen Gupta, A., Benthuysen, J. A., Deser, C., Frölicher, T. L., et al. (2024). A global overview of marine heatwaves in a changing climate. *Communications Earth & Environment, 5*(1), 701.

Cavole, L. M., Demko, A. M., Diner, R. E., Giddings, A., Koester, I., Pagniello, C. M., et al. (2016). Biological impacts of the 2013–2015 warm-water anomaly in the Northeast Pacific: winners, losers, and the future. *Oceanography, 29*(2), 273-285.

Cervantes, B. T., Fewings, M. R., & Risien, C. M. (2024). Subsurface temperature anomalies off Central Oregon during 2014–2021. *Journal of Geophysical Research: Oceans, 129*(10), e2023JC020565.

Chen, T. C., Kahru, M., Landry, M. R., Ohman, M. D., Thompson, A. R., & Stukel, M. R. (2024). Multi-Trophic Level Responses to Marine Heatwave Disturbances in the California Current Ecosystem. *Ecology Letters, 27*(12), e14502.

Cloern, J. E. (1999). The relative importance of light and nutrient limitation of phytoplankton growth: a simple index of coastal ecosystem sensitivity to nutrient enrichment. *Aquatic ecology, 33*, 3-15.

Closset, I., McNair, H. M., Brzezinski, M. A., Krause, J. W., Thamatrakoln, K., & Jones, J. L. (2021). Diatom response to alterations in upwelling and nutrient dynamics associated with climate forcing in the California Current System. *Limnology and Oceanography, 66*(4), 1578-1593.

Cordero-Quirós, N., Miller, A. J., Pan, Y., Balitaan, L., Curchitser, E., & Dussin, R. (2022). Physical-Ecological Response of the California Current System to ENSO events in ROMS-NEMURO. *Ocean Dynamics, 72*, 21-36.

Cordero-Quirós, N., Miller, A. J., Subramanian, A. C., Luo, J. Y., & Capotondi, A. (2019). Composite physical–biological El Niño and La Niña conditions in the California

642   Current System in CESM1-POP2-BEC. *Ocean Modelling, 142*, 101439.

643 Cullen, J. J. (2015). Subsurface chlorophyll maximum layers: enduring enigma or mystery
644   solved? *Annual review of marine science, 7*(1), 207-239.

645 Dalsin, M., Walter, R. K., & Mazzini, P. L. (2023). Effects of basin-scale climate modes and
646   upwelling on nearshore marine heatwaves and cold spells in the California Current.
647   *Scientific Reports, 13*(1), 12389.

648 Delgadillo-Hinojosa, F., Félix-Bermúdez, A., Torres-Delgado, E. V., Durazo, R., Camacho-
649   Ibar, V., Mejía, A., et al. (2020). Impacts of the 2014–2015 warm-water anomalies
650   on nutrients, chlorophyll-a and hydrographic conditions in the coastal zone of
651   northern Baja California. *Journal of Geophysical Research: Oceans, 125*(12),
652   e2020JC016473.

653 Di Lorenzo, E., & Mantua, N. (2016). Multi-year persistence of the 2014/15 North Pacific
654   marine heatwave. *Nature Climate Change, 6*(11), 1042-1047.

655 Eakin, C. M., Sweatman, H. P., & Brainard, R. E. (2019). The 2014–2017 global-scale coral
656   bleaching event: insights and impacts. *Coral Reefs, 38*(4), 539-545.

657 Falkowski, P. G., Fenchel, T., & Delong, E. F. (2008). The microbial engines that drive Earth's
658   biogeochemical cycles. *Science, 320*(5879), 1034-1039.

659 Fernández-González, C., Tarran, G. A., Schuback, N., Woodward, E. M. S., Arístegui, J., &
660   Marañón, E. (2022). Phytoplankton responses to changing temperature and
661   nutrient availability are consistent across the tropical and subtropical Atlantic.
662   *Communications Biology, 5*(1), 1035.

663 Fewings, M. R., & Brown, K. S. (2019). Regional structure in the marine heat wave of
664   summer 2015 off the western United States. *Frontiers in Marine Science, 6*, 564.

665 Fischer, A. D., Houliez, E., Bill, B. D., Kavanaugh, M. T., Alin, S. R., Collins, A. U., et al. (2024).
666   Nutrient limitation dampens the response of a harmful algae to a marine
667   heatwave in an upwelling system. *Limnology and Oceanography*.

668 Franks, P. J., Di Lorenzo, E., Goebel, N. L., Chenillat, F., Rivière, P., EDWARDS, C. A., & Miller,
669   A. J. (2013). Modeling physical-biological responses to climate change in the
670   California Current System. *Oceanography, 26*(3), 26-33.

671 Frölicher, T. L., Fischer, E. M., & Gruber, N. (2018). Marine heatwaves under global
672   warming. *Nature, 560*(7718), 360-364.

673 Frölicher, T. L., & Laufkötter, C. (2018). Emerging risks from marine heat waves. *Nature*
674   *communications, 9*(1), 650.

675 Gomes, D. G., Ruzicka, J. J., Crozier, L. G., Huff, D. D., Phillips, E. M., Hernvann, P.-Y., et al.
676   (2024). An updated end-to-end ecosystem model of the northern California
677   Current reflecting ecosystem changes due to recent marine heatwaves. *PLoS One,*
678   *19*(1), e0280366.

679 Gruber, N., Boyd, P. W., Frölicher, T. L., & Vogt, M. (2021). Biogeochemical extremes and
680   compound events in the ocean. *Nature, 600*(7889), 395-407.

681 Hauri, C., Pagès, R., Hedstrom, K., Doney, S. C., Dupont, S., Ferriss, B., & Stuecker, M. F.
682   (2024). More than marine heatwaves: a new regime of heat, acidity, and low
683   oxygen compound extreme events in the Gulf of Alaska. *AGU Advances, 5*(1),
684   e2023AV001039.

Hayashida, H., Matear, R. J., & Strutton, P. G. (2020). Background nutrient concentration determines phytoplankton bloom response to marine heatwaves. *Global change biology, 26*(9), 4800-4811.

Hobday, A. J., Alexander, L. V., Perkins, S. E., Smale, D. A., Straub, S. C., Oliver, E. C., et al. (2016). A hierarchical approach to defining marine heatwaves. *Progress in oceanography, 141*, 227-238.

Holbrook, N. J., Scannell, H. A., Sen Gupta, A., Benthuysen, J. A., Feng, M., Oliver, E. C., et al. (2019). A global assessment of marine heatwaves and their drivers. *Nature communications, 10*(1), 2624.

Hu, Q., Chen, X., He, X., Bai, Y., Zhong, Q., Gong, F., et al. (2022). Seasonal variability of phytoplankton biomass revealed by satellite and BGC-Argo data in the central tropical Indian Ocean. *Journal of Geophysical Research: Oceans, 127*(10), e2021JC018227.

Iglesias, I. S., Fiechter, J., Santora, J. A., & Field, J. C. (2024). Vertical distribution of mesopelagic fishes deepens during marine heatwave in the California Current. *ICES Journal of Marine Science, 81*(9), 1837-1849.

Kavanaugh, M. T., Nielsen, K. J., Chan, F. T., Menge, B. A., Letelier, R. M., & Goodrich, L. M. (2009). Experimental assessment of the effects of shade on an intertidal kelp: do phytoplankton blooms inhibit growth of open coast macroalgae? *Limnology and Oceanography, 54*(1), 276-288.

Köhn, E. E., Vogt, M., Münnich, M., & Gruber, N. (2024). On the vertical structure and propagation of marine heatwaves in the Eastern Pacific. *Journal of Geophysical Research: Oceans, 129*(1), e2023JC020063.

Landry, M. R., Freibott, A. L., Beatty, J. L., & Selph, K. E. (2024). Phytoplankton biomass responses to a marine heat wave align with altered nitracline depth. *Limnology and Oceanography, 69*(8), 1683-1694.

Landry, M. R., Freibott, A. L., Stukel, M. R., Selph, K. E., Allen, A. E., & Rabines, A. (2024). Phytoplankton growth and grazing dynamics during anomalous heat wave and suppressed upwelling conditions in the southern California Current. *Deep Sea Research Part I: Oceanographic Research Papers, 210*, 104353.

Le Grix, N., Burger, F. A., & Frölicher, T. L. (2025). Surface and subsurface compound marine heatwave and biogeochemical extremes under Climate change. *Global Biogeochemical Cycles, 39*(5), e2025GB008514.

Le Grix, N., Zscheischler, J., Laufkötter, C., Rousseaux, C. S., & Frölicher, T. L. (2020). Compound high temperature and low chlorophyll extremes in the ocean over the satellite period. *Biogeosciences Discussions, 2020*, 1-26.

Lengaigne, M., Menkes, C., Aumont, O., Gorgues, T., Bopp, L., André, J.-M., & Madec, G. (2007). Influence of the oceanic biology on the tropical Pacific climate in a coupled general circulation model. *Climate Dynamics, 28*(5), 503-516.

Liang, S., & Wang, D. (2017). Moderate resolution imaging spectroradiometer (MODIS) downward shortwave radiation (MCD18A1) and photosynthetically active radiation (MCD18A2) algorithm theoretical basis document. In *Google Scholar There is no Corresponding Record for This Reference*.

728 Marañón, E. (2015). Cell size as a key determinant of phytoplankton metabolism and
729   community structure. *Annual review of marine science, 7*(1), 241-264.
730 McCabe, R. M., Hickey, B. M., Kudela, R. M., Lefebvre, K. A., Adams, N. G., Bill, B. D., et al.
731   (2016). An unprecedented coastwide toxic algal bloom linked to anomalous
732   ocean conditions. *Geophysical Research Letters, 43*(19), 10,366-310,376.
733 McClatchie, S., Goericke, R., Leising, A., Auth, T. D., Bjorkstedt, E., Robertson, R. R., et al.
734   (2016). State of the California current 2015-16: comparisons with the 1997-98 El
735   Nino.
736 Mélin, F., Vantrepotte, V., Chuprin, A., Grant, M., Jackson, T., & Sathyendranath, S. (2016).
737   *Global trends in chlorophyll concentration observed with the satellite ocean
738   colour data record.* Paper presented at the Living Planet Symposium.
739 Miller, A. J., Song, H., & Subramanian, A. C. (2015). The physical oceanographic
740   environment during the CCE-LTER Years: Changes in climate and concepts. *Deep
741   Sea Research Part II: Topical Studies in Oceanography, 112*, 6-17.
742 Moreira-Coello, V., Mouriño-Carballido, B., Marañón, E., Fernández-Carrera, A., Bode, A.,
743   & Varela, M. M. (2017). Biological N2 fixation in the upwelling region off NW Iberia:
744   magnitude, relevance, and players. *Frontiers in Marine Science, 4*, 303.
745 Mouriño-Carballido, B., Otero Ferrer, J. L., Fernández Castro, B., Marañón, E., Blazquez
746   Maseda, M., Aguiar-Gonzalez, B., et al. (2021). Magnitude of nitrate turbulent
747   diffusion in contrasting marine environments. *Scientific Reports, 11*(1), 18804.
748 Myers, T. A., Mechoso, C. R., Cesana, G. V., DeFlorio, M. J., & Waliser, D. E. (2018). Cloud
749   feedback key to marine heatwave off Baja California. *Geophysical Research Letters,
750   45*(9), 4345-4352.
751 Noh, K. M., Lim, H.-G., & Kug, J.-S. (2022). Global chlorophyll responses to marine
752   heatwaves in satellite ocean color. *Environmental Research Letters, 17*(6), 064034.
753 Ohman, M. D., Barbeau, K., Franks, P. J., Goericke, R., Landry, M. R., & Miller, A. J. (2013).
754   Ecological transitions in a coastal upwelling ecosystem. *Oceanography, 26*(3),
755   210-219.
756 Oliver, E. C., Benthuysen, J. A., Darmaraki, S., Donat, M. G., Hobday, A. J., Holbrook, N. J.,
757   et al. (2021). Marine heatwaves. *Annual review of marine science, 13*(1), 313-342.
758 Oliver, E. C., Donat, M. G., Burrows, M. T., Moore, P. J., Smale, D. A., Alexander, L. V., et al.
759   (2018). Longer and more frequent marine heatwaves over the past century.
760   *Nature communications, 9*(1), 1324.
761 Peña, M. A., Nemcek, N., & Robert, M. (2019). Phytoplankton responses to the 2014–2016
762   warming anomaly in the northeast subarctic Pacific Ocean. *Limnology and
763   Oceanography, 64*(2), 515-525.
764 Plume, G., Walter, R. K., Cobb, I., Dalsin, M., Mazzini, P. L., Shunk, N. P., et al. (2025).
765   Vertical structure of subsurface marine heatwaves in a shallow nearshore
766   upwelling system. *Scientific Reports, 15*(1), 6353.
767 Ren, X., Liu, W., Capotondi, A., Amaya, D. J., & Holbrook, N. J. (2023). The Pacific Decadal
768   Oscillation modulated marine heatwaves in the Northeast Pacific during past
769   decades. *Communications Earth & Environment, 4*(1), 218.
770 Reynolds, R. W., Smith, T. M., Liu, C., Chelton, D. B., Casey, K. S., & Schlax, M. G. (2007).

771   Daily high-resolution-blended analyses for sea surface temperature. *Journal of*
772   *climate, 20*(22), 5473-5496.

773   Rykaczewski, R. R., & Dunne, J. P. (2010). Enhanced nutrient supply to the California
774   Current Ecosystem with global warming and increased stratification in an earth
775   system model. *Geophysical Research Letters, 37*(21).

776   Shigesada, N., & Okubo, A. (1981). Analysis of the self-shading effect on algal vertical
777   distribution in natural waters. *Journal of Mathematical Biology, 12*, 311-326.

778   Shiozaki, T., Fujiwara, A., Sugie, K., Nishino, S., Makabe, A., & Harada, N. (2022). Bottom-
779   associated phytoplankton bloom and its expansion in the Arctic Ocean. *Global*
780   *change biology, 28*(24), 7286-7295.

781   Smale, D. A., Wernberg, T., Oliver, E. C., Thomsen, M., Harvey, B. P., Straub, S. C., et al.
782   (2019). Marine heatwaves threaten global biodiversity and the provision of
783   ecosystem services. *Nature Climate Change, 9*(4), 306-312.

784   Smith, K. E., Burrows, M. T., Hobday, A. J., King, N. G., Moore, P. J., Sen Gupta, A., et al.
785   (2023). Biological impacts of marine heatwaves. *Annual review of marine science,*
786   *15*(1), 119-145.

787   Smith, K. E., Burrows, M. T., Hobday, A. J., Sen Gupta, A., Moore, P. J., Thomsen, M., et al.
788   (2021). Socioeconomic impacts of marine heatwaves: Global issues and
789   opportunities. *Science, 374*(6566), eabj3593.

790   Smith, K. E., Gupta, A. S., Amaya, D., Benthuysen, J. A., Burrows, M. T., Capotondi, A., et al.
791   (2025). Baseline matters: Challenges and implications of different marine
792   heatwave baselines. *Progress in oceanography, 231*, 103404.

793   Stone, H. B., Banas, N. S., MacCready, P., Kudela, R. M., & Ovall, B. (2020). Linking
794   chlorophyll concentration and wind patterns using satellite data in the central and
795   northern california current system. *Frontiers in Marine Science, 7*, 551562.

796   Thomas, M. K., Kremer, C. T., Klausmeier, C. A., & Litchman, E. (2012). A global pattern of
797   thermal adaptation in marine phytoplankton. *Science, 338*(6110), 1085-1088.

798   Viljoen, J. J., Sun, X., & Brewin, R. J. (2024). Climate variability shifts the vertical structure
799   of phytoplankton in the Sargasso Sea. *Nature Climate Change, 14*(12), 1292-1298.

800   Wei, X., Li, K. Y., Kilpatrick, T., Wang, M., & Xie, S. P. (2021). Large-scale conditions for the
801   record-setting Southern California marine heatwave of August 2018. *Geophysical*
802   *Research Letters, 48*(7), e2020GL091803.

803   Wernberg, T., Smale, D. A., Tuya, F., Thomsen, M. S., Langlois, T. J., De Bettignies, T., et al.
804   (2013). An extreme climatic event alters marine ecosystem structure in a global
805   biodiversity hotspot. *Nature Climate Change, 3*(1), 78-82.

806   Wong, J., Münnich, M., & Gruber, N. (2024). Column-compound extremes in the global
807   ocean. *AGU Advances, 5*(3), e2023AV001059.

808   Wyatt, A. M., Resplandy, L., & Marchetti, A. (2022). Ecosystem impacts of marine heat
809   waves in the northeast Pacific. *Biogeosciences, 19*(24), 5689-5705.

810   Yuan, T., Zhang, J., Yang, S., Su, Q., Zhao, Z., & Ren, K. (2024). Vertical structures of marine
811   heatwaves in the South China Sea: Characteristics, drivers and impacts on
812   chlorophyll concentration. *Journal of Geophysical Research: Oceans, 129*(12),
813   e2024JC021091.

814 Zaba, K. D., & Rudnick, D. L. (2016). The 2014–2015 warming anomaly in the Southern
815   California Current System observed by underwater gliders. *Geophysical Research*
816   *Letters, 43*(3), 1241-1248.

817 Zaba, K. D., Rudnick, D. L., Cornuelle, B. D., Gopalakrishnan, G., & Mazloff, M. R. (2020).
818   Volume and heat budgets in the coastal California current system: Means, annual
819   cycles, and interannual anomalies of 2014–16. *Journal of Physical Oceanography,*
820   *50*(5), 1435-1453.

821 Zhan, W., Feng, M., Zhang, Y., Shen, X., Zhan, H., & He, Q. (2024). Reduced and smaller
822   phytoplankton during marine heatwaves in eastern boundary upwelling systems.
823   *Communications Earth & Environment, 5*(1), 629.

824 Zhan, W., Zhang, Y., He, Q., & Zhan, H. (2023). Shifting responses of phytoplankton to
825   atmospheric and oceanic forcing in a prolonged marine heatwave. *Limnology and*
826   *Oceanography, 68*(8), 1821-1834.

827 Zhang, Y., Du, Y., Feng, M., & Hobday, A. J. (2023). Vertical structures of marine heatwaves.
828   *Nature communications, 14*(1), 6483.

829 Zheng, J., Xiu, P., Zeng, L., Zhu, X., Ji, X., Gao, S., & Li, Z. (2024). Phytoplankton response
830   to the record-breaking marine heatwave in the summer of 2020 in the South
831   China Sea. *Journal of Geophysical Research: Oceans, 129*(10), e2024JC021275.

832 Stukel, R. M., Allen, E. A., Barbeau, A. K., Chabert, P., Dovel, S., Gangrade, S., Kranz, A. S., Lampe,
833   H. R., Landry, R. M., Marrec, P., Messié, M., Miller, J. A., Ohman, D. M., Wilkinson, G.
834   (2025). Disturbance ecology in a pelagic upwelling biome: Lagrangian frameworks for
835   studying succession. In prep for: *Bioscience* special issue on Long-Term Change in Eastern
836   Boundary Current Upwelling Biomes

Acknowledgments

Author contributions

J.L. and A.M designed the study. J.L conducted the analyses and wrote the first draft of the
manuscript under A.M.'s instruction. D.A., P.B. and Q.W. were involved in improving the
manuscript. Y.G. and P.L. provided fundings for the study.

848 **Competing interests**

849 The authors declare no competing interests.